

An Experimental Study of Dynamic Delamination of Thick Fiber Reinforced Polymeric Matrix Composites

by J. Lambros and A. J. Rosakis

ABSTRACT—Dynamic delamination of thick fiber reinforced polymeric matrix composite laminates is investigated using optical techniques and high-speed photography. The laminates used in this work are graphite/epoxy fiber reinforced, 65 percent fiber volume fraction, composite plates consisting of 48 plies (6 mm plate thickness). Two different laminate layups are tested: a quasi-isotropic arrangement and a unidirectional arrangement. The experimental setup consists of 152 mm x 152 mm square plates impact loaded in an out-of-plane configuration using a high-speed gas gun. Impact speeds range from 1 m/s to 30 m/s. Real-time imaging of the laminate out-of-plane displacement is performed using the lateral shearing interferometer of coherent gradient sensing (CGS) in conjunction with high-speed photography. Onset of dynamic delamination can be observed, and quantities such as delamination speeds (in some cases up to 1800 m/s) are measured and reported. A brief comparison is made with dynamic fracture experiments of the same material conducted in a separate study.

Introduction

The motivation behind this study is the proposed use of polymeric composite laminates in the construction of submersibles. It is widely known that a very common mode of failure of composite laminates is ply delamination. In service situations delamination will, more often than not, occur in a dynamic fashion, usually triggered by some sudden structural overload (e.g., foreign object impact). In the case of submersible vehicles, the dynamic delamination behavior of the composite will most likely be severely affected by the high hydrostatic compression loading to which the submersible is subjected.

The research we are presently conducting focuses on the real-time visualization of dynamic delamination damage of thick composite laminates that are subjected to an out-of-plane impact. In a laboratory environment, we planned to simulate the high hydrostatic pressure by applying a confining pressure all around the specimen. All results presented in this paper, however, are concerned only with out-of-plane impact of unconfined plates; i.e., no pressure was applied. The optical method used for real-time visualization was the newly developed full-field optical method of coherent gradient sensing (CGS) in reflection.¹ Imaging was performed using a rotating mirror type high-speed camera.

J. Lambros is Assistant Professor, Department of Mechanical Engineering, University of Delaware Newark, DE 19716. A. J. Rosakis is Professor, Graduate Aeronautical Laboratories, California Institute of Technology, Pasadena, CA 91125.

Original manuscript submitted: October 31, 1996.

Final manuscript received: April 8, 1997.

In the past, very few studies have dealt with real-time imaging of dynamic delamination in composites. Chai and coworkers,^{2,3} using the shadow Moiré technique, performed optical measurements on composites subjected to low-velocity out-of-plane impact. More recently, Epstein, Deason and Abdallah⁴ used dynamic Moiré interferometry to measure the deflection of impacted composite plates. Zhu, Goldsmith and Dharan⁵ photographed very high speed projectiles penetrating Kevlar laminates. In the above studies, the framing periods used were between 10 μ s and 50 μ s. This would not allow detailed scrutiny of the early stages of the nucleation and growth of delamination damage. Nevertheless, the above studies represent a very important contribution as they are, to our knowledge, the only ones that perform real-time visualization of impact in composites.

There exist numerous studies of laminate impact in the open literature that are of a theoretical and/or numerical nature.^{6,7} However, most experimental studies in the past have employed postmortem observation of the impacted specimens and have made use of quantities such as final delamination area and impact energy measured before impact to reach their conclusions.^{8,9} Other than the contributions mentioned in the previous paragraph, real-time collection of data during the dynamic propagation of delaminations in composites was made using either strain gages or high-speed acoustic sensors. These methods provide point and/or spatially averaged measurements only.¹⁰ Our aim in this paper is to provide evidence of the feasibility of the use of CGS interferometry for imaging dynamic deformation of composite laminates and to visualize the very early stages of delamination growth in thick polymeric composite laminates subjected to low and intermediate speed impact (1-30 m/s). The novelty of the experimental results presented here is not only that they provide real-time, full-field information about the delaminating composite but that they do so at relatively fast framing rates (approximately 1.7 μ s/frame).

Experimental Setup and Description

The Optical Method of CGS in Reflection

Consider a planar wave front normally incident on an optically flat and specularly reflective surface of a mechanically isotropic opaque plate. The undeformed specimen surface occupies the (x_1, x_2) plane (see Fig. 1). After impact, the specimen surface deforms and acquires an out-of-plane displacement $u_3(x_1, x_2)$. Incident parallel rays reflected from the deformed specimen surface will deviate from parallelism after reflection. In this situation, the reflected wave front

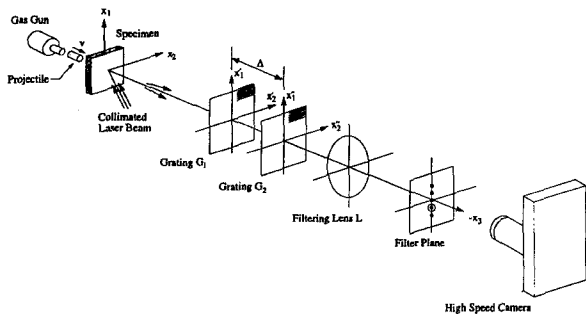


Fig. 1—Schematic of the reflection CGS interferometer for use in dynamic delamination studies

will no longer be planar. The CGS setup, described below, is used to provide full-field information about the amount of deviation from parallelism of each reflected ray. It is then possible¹¹ to relate the resulting interferograms with the slope of the out-of-plane displacement u_3 .

A schematic of the experimental apparatus is shown in Fig. 1. When the rays are reflected from the specimen, they are processed by a pair of high-density gratings G_1 and G_2 separated a distance Δ apart (typically 40 mm). In a typical setup, the gratings have their rulings parallel to either the x_1 - or x_2 -direction. The grating pitch is denoted by p , which is equal to 0.0254 mm in these experiments (i.e., 40 lines/mm). The action of the gratings is to displace (shear) the reflected beam and recombine it with itself, thus creating an interferogram after G_2 . The light emerging from G_2 is collected by the filtering lens L , and its frequency content (diffraction spots) is displayed on its back focal plane. By locating a filtering aperture around either the ± 1 diffraction orders, information regarding the gradient components of out-of-plane displacement u_3 along either the x_1 - or x_2 -axis is obtained on the image plane. The camera is kept focused on the specimen surface. For grating rulings perpendicular to the x_α -axis, the resulting fringe pattern is proportional to $\partial(u_3)/\partial x_\alpha$, $\alpha = (1, 2)$.

More specifically, and as demonstrated by a first-order analysis¹ or a higher order Fourier optics analysis,¹² the resulting bright fringes can be related to gradients of u_3 as follows:

$$\frac{\partial(u_3)}{\partial x_\alpha} = \frac{k_\alpha p}{2\Delta} \quad \alpha = (1, 2) \quad (1)$$

$$k_\alpha = \begin{cases} m & \text{for } \alpha = 1, m = 0, \pm 1, \pm 2, \dots \\ n & \text{for } \alpha = 2, n = 0, \pm 1, \pm 2, \dots \end{cases}$$

where m and n are the fringe orders for the x_1 , x_2 gradient contours, respectively.

Experimental Apparatus and Procedure

The particular composite chosen for this study was a graphite/epoxy system, with 33 msi (230 GPa) fibers and 65 percent fiber volume ratio. The in-plane dimensions of the plates used were 152 mm by 152 mm. Two different layups were used for the laminates. The first had the following

stacking sequence

$$[45/0/ - 45/90/90/ - 45/0/45/45/0/ \\ - 45/90/90/ - 45/0/45/45/0/ \\ - 45/90/90/ - 45/0/45/]_s.$$

This is a total of 48 plies, which yield a composite plate of 6 mm thickness. (Although not thick in terms of a submersible structure, these composites are thicker than those commonly used in aviation applications.) The above stacking sequence produces a quasi-isotropic plate (in the in-plane directions) that also has no axial-bending coupling. To keep the laminate thickness fixed but to simplify subsequent data analysis, the second configuration tested was a unidirectional layup of a total of 48 plies. The most crucial aspect of specimen preparation was to obtain at least one surface that was optically flat and specularly reflective. This was achieved by curing the composite under pressure against an optically flat tool (such as a thick glass substrate, for example). The optically flat composite plates were provided by Composite Mirror Applications Inc. (Tucson, AZ, USA). Subsequently, the specimens were coated in-house using a vacuum deposition chamber.

Each composite plate was loaded by means of a gas gun as shown in Fig. 1. Impact occurred on the back surface of the composite plate. A projectile was fired onto the plate at speeds between 1 m/s and 30 m/s. The projectile was made of steel and was 80 mm in length and 25 mm in diameter, tapering to a rounded point. After loading, compressive waves travel the thickness of the plate and reflect as tension. As time progresses, wave reflections from, and delaminations of, each layer contribute to the deformation. The combined effects of each deforming layer manifest themselves as a changing out-of-plane deformation on the front (mirrored) surface of the composite plate. The reflection CGS technique in conjunction with high-speed photography was used to record slope components of the out-of-plane deformation field of the front surface in real time. The light source used for specimen illumination was a Spectra-Physics argon ion pulse laser (model 166-09). Two fine diffraction gratings (40 lines/mm) were used to provide optical differentiation of the resultant distorted beam. A rotating mirror high-speed camera (Cordin model 330A) was used for imaging. It is capable of running at framing rates of up to 2 million frames/s. In the current tests, it was run at a framing rate of 600,000 frames/s (i.e., 1.7 μ s/frame). By using short laser pulses of 30 ns duration, we were able to freeze the fast-changing deformation and thus produce sharp interference patterns. The laser pulsing was triggered by a strain gage on the specimen that sensed the impact of the projectile.

Feasibility of the CGS Method

Before proceeding with actual dynamic experiments, we decided to test the feasibility of using the CGS technique in reflection for capturing delamination of composite laminates. The present study is the first time this newly developed optical method was to be used in such a situation. Investigation of the feasibility of the method consisted of performing postmortem optical observations of impacted composite plates. A plate was impacted in an out-of-plane fashion with a projectile traveling at 1 m/s. Subsequently, the residual deformation of the laminate was imaged by means of a static CGS setup. This is the same setup as in Fig. 1, but with the imaging medium being a regular 35-mm SLR camera. CGS

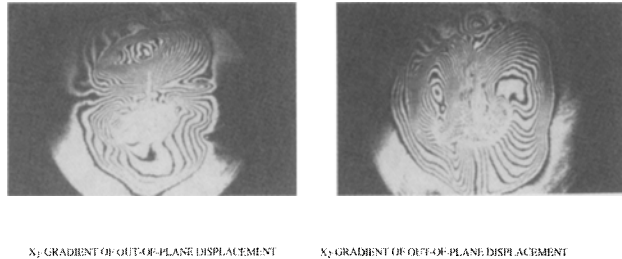


Fig. 2—Postmortem CGS interferograms showing (a) the x_1 -slope and (b) the x_2 -slope of a quasi-isotropic composite laminate impacted at 1 m/s in an out-of-plane configuration. The x_1 -axis is in the horizontal direction. The total field of view is 50 mm

interferograms showing both the x_1 and x_2 derivatives of the out-of-plane displacement u_3 of the mirrored surface (opposite from the impact site) can be seen in Fig. 2. We can see that the fringe contrast is very good, and the different regions of the deformation are clearly distinguishable. The images presented in Fig. 2 do indeed prove that the optical technique of CGS is capable of imaging the postmortem deformation fields created by composite plate delamination. From this figure, it is also clear that the residual deformation field is rather complicated. It would be very difficult to quantitatively analyze the fringe patterns seen in Fig. 2 using eq (1). Nevertheless, some qualitative conclusions can be drawn.

The field of view, which is the size of the laser beam used, is 50 mm. The fringe patterns visible cover almost the whole 50-mm area of the beam. We can clearly see that there is a large extent of severe out-of-plane deformation. It is worth noting at this point that when observing the damaged plate with the naked eye, the apparent extent of damage was significantly less than 50 mm.

There are several distinct regions in the fringe pattern that have a large concentration of fringes over a small distance. It is believed that these are boundaries that enclose areas of delamination inside the composite. These delamination fronts are internal to the composite, and not all are necessarily between the same pair of layers. In all cases, however, the effect is seen as a net out-of-plane deformation of the uppermost layer. The fact that it is possible to have multiple delaminations at various depths inside the plate makes quantitative use of experimental information contained in the interferograms even harder. In the dynamic experiments, however, when using fast framing rates, we would be able to capture the very early stages of delamination between the two topmost layers only.

Observations and Results

Low-speed Impact of Quasi-isotropic Laminates

A selected sequence of x_2 -slope interferograms from a 1-m/s impact speed experiment is shown in Fig. 3. These are 6 selected interferograms from a total number of 80 recorded. The framing rate used for this test was 1.7 μ s/frame, but as can be seen in Fig. 3, there is no significant amount of deformation until 20 μ s–30 μ s after impact. The field of view in this test is 50 mm, and the x_2 -direction is coincident with the vertical direction of the page. The deformation spread to about 50 mm in around 40 μ s. This is, relatively speaking, a

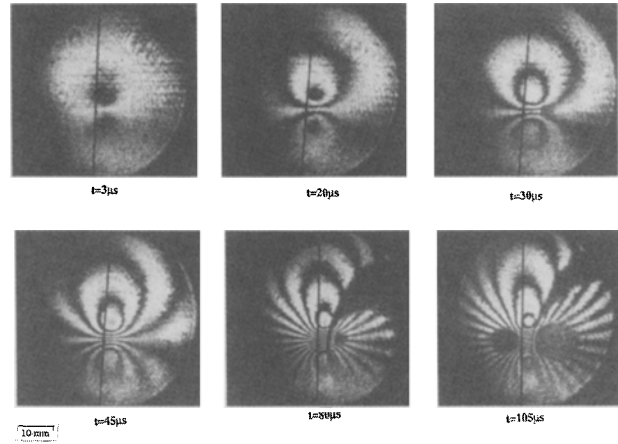


Fig. 3—Selected sequence of dynamic CGS interferograms showing deformation of a quasi-isotropic composite laminate impacted at 1 m/s

long time. A dilatational wave traveled the thickness of the specimen about 15 times in this time interval. (The through thickness dilatational wave speed for this laminate was measured at 2480 m/s using ultrasonic measurements.) As time progresses, the delamination spreads, and by 105 μ s it reaches a significant portion of the specimen. Even so, it is clear that the interferograms captured in the dynamic experiment are very much simpler in nature than the interferograms depicting residual damage shown in Fig. 2. The reason is that the dynamic test is actually imaging the very first delamination that occurs.

The shape of the fringe pattern in Fig. 3 at each time is self similar. The simplicity of the pattern makes it possible to easily extract numerical information about the progression of delamination in a test such as that of Fig. 3. Analysis can be performed by digitizing each fringe, both dark and bright, to obtain x_1 , x_2 values of each contour of constant x_2 -slope. The bottom lobe denotes a positive slope (increasing u_3), and the upper lobe denotes a negative slope (decreasing u_3). Maximum out-of-plane displacement occurs in the center of the field of view of the interferogram ($x_1 = 0$, $x_2 = 0$) directly across from the impact site and corresponds to a fringe order of zero. All bright fringes have an integer order (constructive interference), whereas all dark fringes have a half-integer (destructive interference). Experimental data in the form x_1 , x_2 , n , where n is the fringe order along each contour (fringe), are subsequently integrated to provide out-of-plane displacement u_3 . Figure 4 shows a time history of the profile of out-of-plane displacement u_3 , only along the x_2 -axis (i.e., for $x_1 = 0$). It can be clearly seen in Fig. 4 how the delamination profile increases with time. The profile is relatively symmetrical around $x_1 = 0$, at least for the time frames involved here. As expected, there is a significant rise in the maximum height of deformation between 20 μ s and 80 μ s. Results from the 105- μ s picture were not plotted on this diagram, since they would be significantly off this scale. One interesting point, however, is that the in-plane extent of delamination does not spread much between 20 μ s and 30 μ s, whereas it spreads significantly after that. This suggests that delamination growth occurs in bursts. By measuring the distance the delamination spreads between 30 μ s and 80 μ s, we are able to obtain an average delamination speed. This is around 500 m/s.

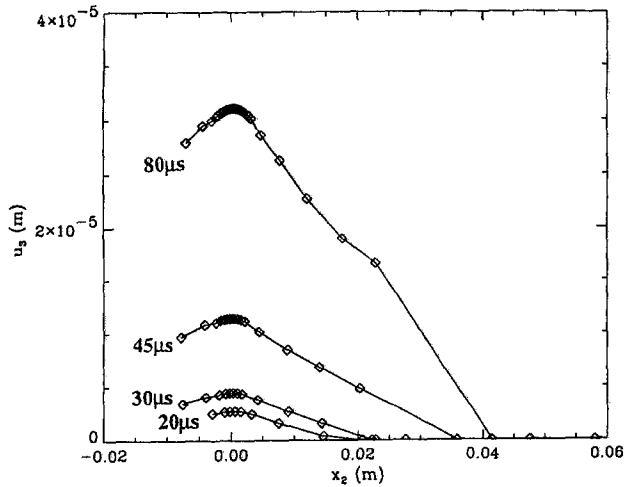


Fig. 4—Profile of the delamination history along $x_1 = 0$ for the test shown in Fig. 3

As seen in the low-impact speed test shown in Fig. 3, it takes a relatively long time, in dynamic terms, for the delamination to spread over a substantial area of the specimen. In this time ($\approx 100\mu\text{s}$), a dilatational wave would have reflected through the thickness of the 6-mm composite plate approximately 30 times. This would be enough for the laminate to start flexural vibrations. These vibrations may substantially affect the progress of damage at later stages of the experiment. Therefore, in an attempt to produce severe delamination at very early stages after impact, it was decided to use impact speeds higher than 1m/s. Results of these tests are discussed in the next section.

Intermediate-speed Impact of Quasi-isotropic Laminates

Figure 5 shows a sequence of interferograms of the x_2 -slope of a composite laminate that has been impacted at 30 m/s. The field of view shown is 20 mm. The fringe patterns appear, qualitatively at least, very similar to those obtained in the low-impact speed experiments. One difference, however, is in the test duration. In a very much shorter time than before, about $20\mu\text{s}$, there is a much larger fringe density. (Both low and intermediate impact speed tests used the same settings of p and Δ for the interferometer and thus had the same sensitivity.) In addition, the field of view in Fig. 5 is smaller than in Fig. 3. This shows that not only is the deformation more intense in the higher impact speed tests, it is much more localized. As the impact speed increases, there is much less time for the composite to respond to the relatively long (80 mm) projectile penetrating it.

Qualitative differences between the fringe patterns of Fig. 5 and those of Fig. 3 start appearing at around $20\mu\text{s}$ after impact. At $21.7\mu\text{s}$, in Fig. 5, there is an additional minimum formed in the fringe pattern. This is visible as a second closed loop of fringes at the top part of each of these frames. A blow up of that region is shown in Fig. 6. There is a clear second minimum of slope visible in Fig. 6 (shown by the arrow). In addition, there are discrete kinks forming in previously smooth fringes. It is believed that this is the front of a second delamination that has occurred under the main (first) delamination. It nucleates in the frame at $21.7\mu\text{s}$ (Fig. 6) and is seen growing in the subsequent frame. By measuring the

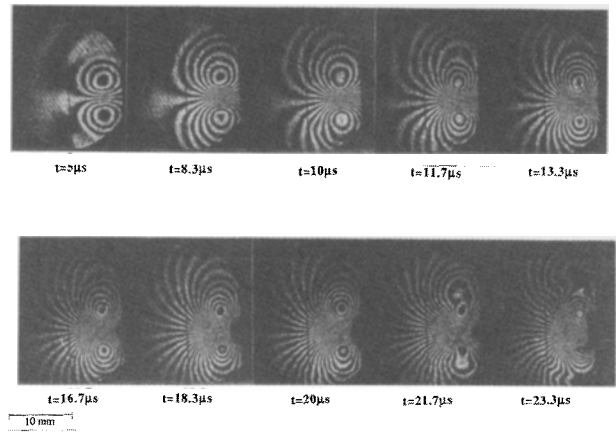


Fig. 5—Sequence of dynamic CGS interferograms showing deformation of a quasi-isotropic composite laminate impacted at 30 m/s.



Fig. 6—Enlarged area from the interferogram at time $21.7\mu\text{s}$ in Fig. 5. The arrow points to the formation of the second negative minimum in the fringe pattern

distance of propagation of this second delamination front, we find that the propagation speed for this delamination is about $1800 \pm 100\text{ m/s}$. This velocity is a significant fraction of the through thickness dilatational wave speed of the composite, thus denoting a very dynamic event.

Quantitative results can be obtained from the interferograms using the procedure outlined in the previous section. When the data obtained from the interferograms are integrated over the entire field of view, we obtain the out-of-plane displacement u_3 . Results from such an integration are visualized in contour form in Figs. 7(a)-(c). Contour levels for the times at $5\mu\text{s}$, $11.7\mu\text{s}$ and $20\mu\text{s}$ are shown from an experiment corresponding to an impact speed of 20 m/s. Contour intervals of $5\mu\text{m}$ are used (with the exception of the first contour, which corresponds to $1\mu\text{m}$ displacement). By comparing the three plots, the increase in the size and extent of deformation is clear. An alternative visualization of the same data is shown in Figs. 8(a)-(c). The previous contour plots have been superimposed onto a three-dimensional visualization of

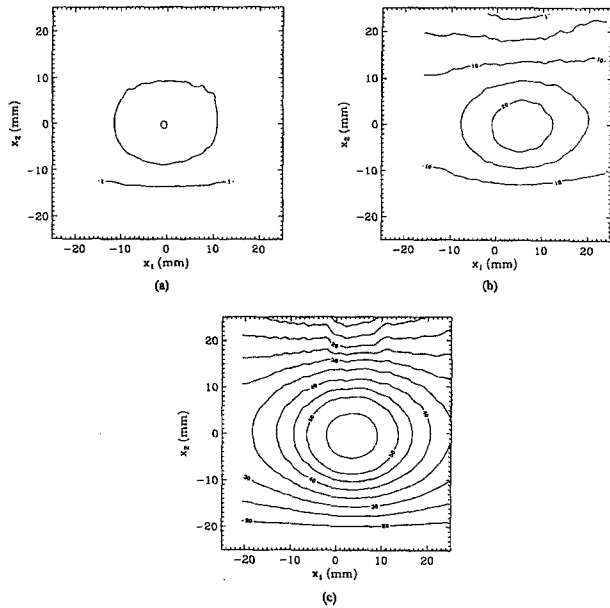


Fig. 7—Contour plots of out-of-plane displacement u_3 for an experiment with impact speed 20 m/s at times of (a) 5 μ s, (b) 11.7 μ s and (c) 20 μ s. Contour levels at 5- μ m intervals are illustrated

the deforming surface. In Figs. 8(a) and 8(b) a delamination bubble is visible. The bubble grows uniformly in size until, at $t = 20 \mu$ s in Fig. 10(c), an abrupt change of slope, resulting from the appearance of a second delamination, becomes visible. (An arrow in the figure points to the location of this abrupt change in slope.) We believe that this is visual evidence of the appearance of the secondary delamination under the initial damage area.

Intermediate speed Impact of Unidirectional Laminates

A selected sequence of CGS interferograms obtained from the out-of-plane impact of a unidirectional graphite/epoxy plate is shown in Fig. 9. The impact speed used in this experiment was 16 m/s. The fringe patterns look qualitatively very similar to those seen earlier in Figs. 3 and 5. The field of view in this case is again 50 mm, and the fibers are in the vertical direction. It is clear from the pictures that there is an elongation of the fringe pattern in the vertical direction, i.e., along the fibers. To some extent, this may be expected because the wave speeds in the fiber direction are much higher than in the direction perpendicular to them. Information is thus carried faster along the fiber direction, so the delamination would be expected to travel faster in that direction. One can measure the velocity of the delamination front along the fiber direction. This is done by measuring the rate at which the outermost fringe grows with time. The result (along the fiber direction) is shown in Fig. 10. The speed of delamination starts out at about 1500 m/s and drops to less than 1000 m/s in a few microseconds. The fact that this speed changes indicates that the observed interferograms do not correspond to wavefront propagation but rather are evidence of elastic and damage-induced (delamination) deformation. In this experiment as well as those depicted earlier in Figs. 3 and 5, the delamination speed is a quantity that increases and decreases over rather small time scales. This can also be seen in Fig. 4, where the intercept of the profile with the x_1 -axis is indicative

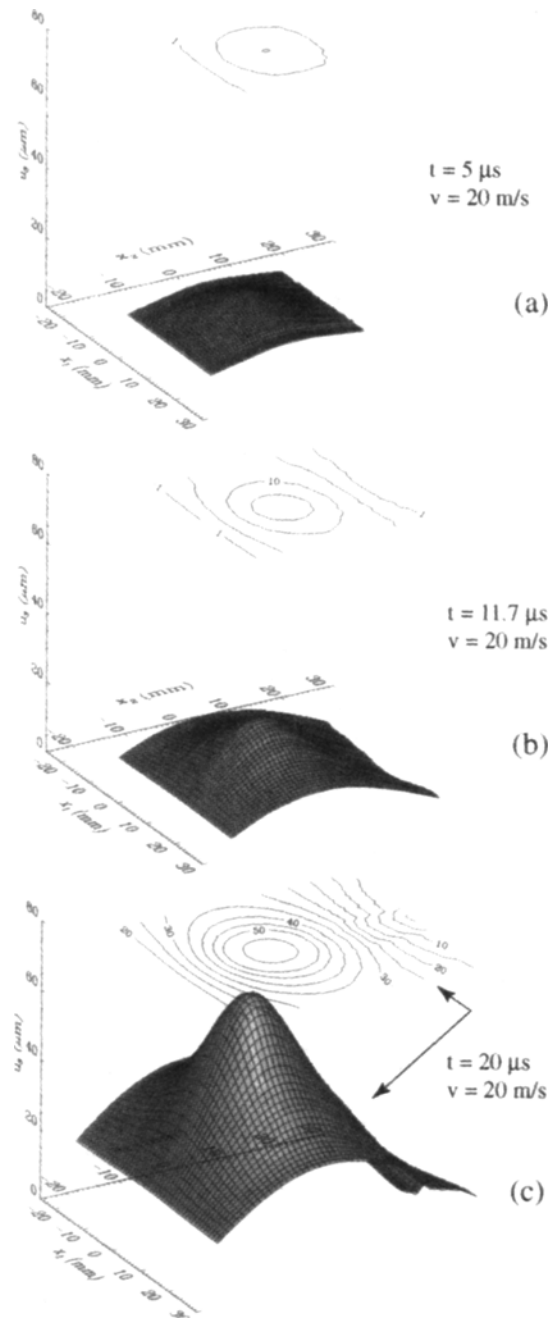


Fig. 8—Time history of the out-of-plane displacement u_3 for an experiment with impact speed 20 m/s at times of (a) 5 μ s, (b) 11.7 μ s and (c) 20 μ s. An arrow points to the appearance of a delamination hump

of delamination speed. It is clear that the speed between 20 μ s and 30 μ s is much less than that between 30 μ s and 45 μ s. Such variations in speed are related to individual stress waves that have reflected either from the specimen surfaces or the multitude of interfaces inside the composite impinging on the growing delamination front. Depending on the particulars of the situation, these stress waves cause a sudden acceleration or deceleration of the delamination front.

Contour representations of the out-of-plane displacement at three different times for the experiment seen in Fig. 9 are

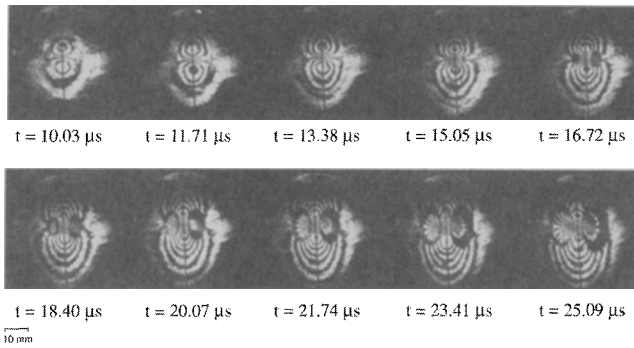


Fig. 9—Sequence of dynamic CGS interferograms showing deformation of a unidirectional composite laminate impacted at 16 m/s. Fibers are in the vertical direction (i.e., parallel to the dark line visible in each frame)

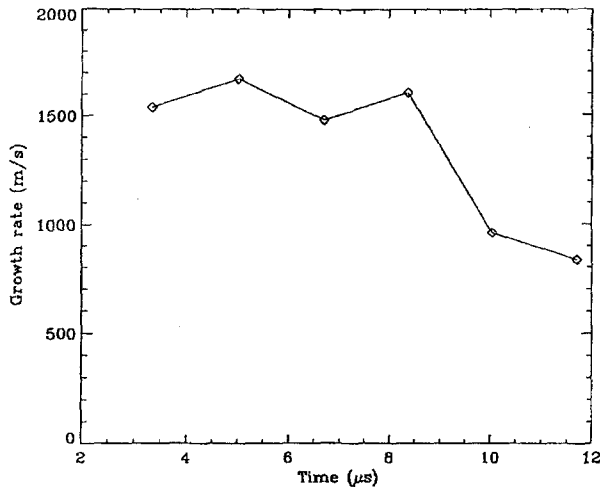


Fig. 10—Velocity history of the out-of-plane delamination front along the fiber direction: impact speed 16 m/s

illustrated in Fig. 11. These results are as expected and show an increase of the delamination both in size and extent. Elongation of deformation along the fiber (x_2) direction is clearly seen. Secondary delaminations do not appear in the unidirectional case because the plate cracks before additional internal delaminations can be generated. When observing the final state of the specimen, it is clear that fracture along the fibers is the main damage mode responsible for failure. (In most unidirectional fiber composites this is expected, since either the matrix or the fiber-matrix interface provides the weakest resistance to failure.) In this experiment, fracture is the predominant mode of failure. Therefore, dynamic delamination and fracture are intimately linked in fiber reinforced composite laminates. For this reason, it is advisable to investigate dynamic fracture of fiber reinforced composite laminates. This subject is briefly discussed in the next section. For more details, the reader is referred to Lambros and Rosakis.¹³

Comparison with Dynamic Fracture Experiments

As part of a separate but related study, experiments to measure dynamic fracture toughness of this material were carried out.¹³ Figure 12 shows a selected sequence of interferograms illustrating dynamic crack growth in a unidirectional

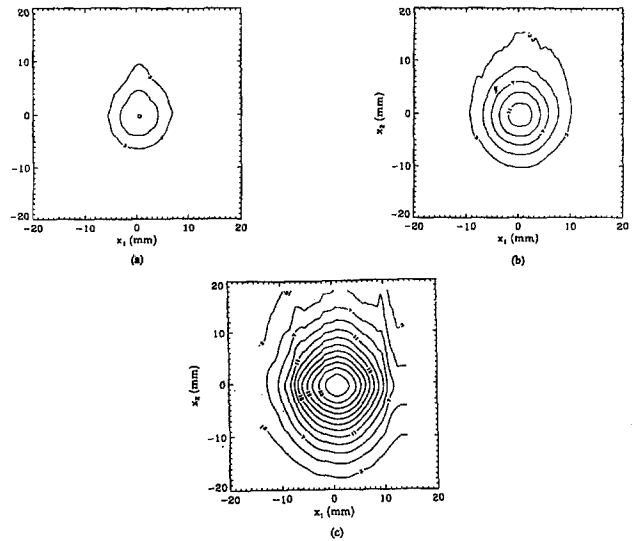


Fig. 11—Contour plots of out-of-plane displacement u_3 for the experiment shown in Fig. 9 at times of (a) 11.7 μ s, (b) 15 μ s and (c) 21.7 μ s. Contour levels at 2- μ m intervals are illustrated

composite system identical to the one used in the delamination experiments. The fiber orientation is along the vertical direction. The current crack tip location is at the point of convergence of all fringes (located along the centerline of each interferogram). The motion of the crack tip is in the vertical direction (i.e., along the fibers) from bottom to top. A stress wave that has been emitted during crack growth is visible. Note that the stress wavefront is not circular, as would be the case in a homogeneous material, but rather is elongated in shape along the fiber direction. This fact is again a consequence of the increased wave speeds in the fiber direction. By measuring the position of the crack tip versus time, it is possible to obtain the crack tip speed. This result is shown in Fig. 13. The crack tip speed increases up to a value of 900 m/s, a value close to the last delamination velocity measurement seen in Fig. 10. This fact may confirm that there is a potential relation between fracture and delamination effects, and therefore eventually criteria, in unidirectional composite plates. In fact, if the composite laminate were perfectly transversely isotropic, there should be no microscopic perceivable difference between a crack or a delamination front. It may be possible to obtain valid dynamic delamination criteria by investigating dynamic fracture of composites.

Conclusions

In this paper, we showed that it is possible to use the optical method of CGS in reflection to provide real-time imaging of delaminated composite plates. Out-of-plane impact experiments at impact speeds of 1 m/s to 30 m/s were performed on quasi-isotropic and unidirectional graphite/epoxy composite laminates. Interferograms for each case were presented and analyzed. By integrating the raw data, it was possible to obtain the real-time variation of the out-of-plane displacement u_3 in each case. Three-dimensional visualization of u_3 was provided. Knowing u_3 , delamination speeds were measured for each case. These speeds ranged from 500 m/s to about 1800 m/s depending on the impact speed and specimen configuration. The possibility of a relation between dynamic fracture and delamination was also discussed.

Acknowledgment

The support of ONR Grant N00014-90-J-1340 is gratefully appreciated.

References

1. Tippur, H.V., Krishnaswamy, S. and Rosakis, A.J., "A Coherent Gradient Sensor for Crack Tip Measurements: Analysis and experimental results," *Int. J. Fract.* **48**, 193–204 (1991).
2. Chai, H., Knauss, W. G. and Babcock, C.D., "Observation of Damage Growth in Compressively Loaded Laminates," *EXPERIMENTAL MECHANICS*, **23**, 329–337 (1983).
3. Chai, H. and Babcock, C.D., "Two Dimensional Modeling of Compressive Failure in Delaminated Composites," *J. Composite Mat.*, **19**, 67–98 (1985).
4. Epstein, J.S., Deason, V.A. and Abdallah, M.G., "Impact Wave Propagation in a Thick Composite Plate Using Dynamic Moiré Interferometry," *Opt. Lasers Eng.*, **17**, 35–46 (1992).
5. Zhu, G., Goldsmith, W. and Dharan, C.K.H., "Penetration of Laminated Kevlar by Projectiles—I. Experimental Investigation," *Int. J. Solids Struct.*, **29**, 399–420 (1992).
6. Mal, A.K. and Lih, S.S., "Elastodynamic Response of a Unidirectional Composite Laminate Subjected to Concentrated Surface Loads: Part I," *J. App. Mech.*, **59**, 878–886 (1992).
7. Lih, S.S. and Mal, A.K., "Elastodynamic Response of a Unidirectional Composite Laminate Subjected to Concentrated Surface Loads: Part II," *J. App. Mech.*, **59**, 887–892 (1992).
8. Cantwell, W.J. and Morton, J., "The Impact Resistance of Composite Material—A Review," *Composites*, **22**, 347–362 (1991).
9. Robinson, P. and Davies, G.A.O., "Impactor Mass and Specimen Geometry Effects in Low Velocity Impact of Laminated Composites," *Int. J. Impact Eng.*, **12**, 189–207 (1992).
10. Daniel, I.M. and Wooh, S.C., "Deformation and Damage of Composite Laminates under Impact Loading," *Impact Response and Elastodynamics of Composites*, eds. A.K. Mal and Y.D. Rajapakse AMD-116 (1989).
11. Rosakis, A.J., "Two optical techniques sensitive to gradients of optical path difference: The method of caustics and the coherent gradient sensor (CGS)," *Experimental Techniques in Fracture III*, ed. J. Epstein, VCH Publishers, New York, 327–425 (1993).
12. Lee, Y.J., Lambros, J. and Rosakis, A.J., "Analysis of Coherent Gradient Sensing (CGS) by Fourier Optics," *Opt. Lasers Eng.*, **25**, 25–53 (1996).
13. Lambros, J. and Rosakis, A.J., "Dynamic Crack Initiation and Growth in Thick Unidirectional Graphite/epoxy Plates," *Composites Sci. Tech.*, **57**, 55–65 (1997).

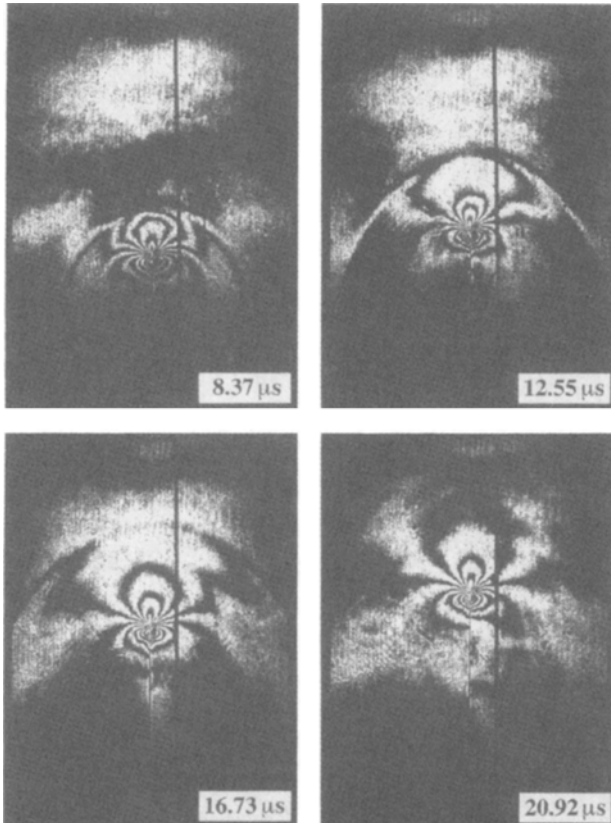


Fig. 12—Sequence of dynamic CGS interferograms showing dynamic crack growth in a unidirectional graphite/epoxy composite laminate impacted at 4 m/s in a drop-weight tower. Crack propagation is along the fiber direction

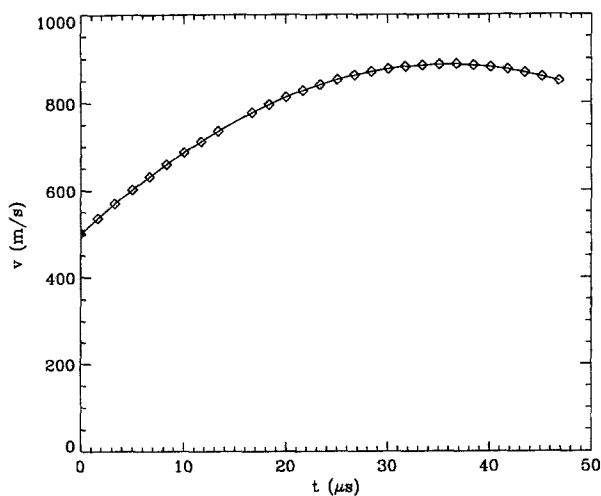


Fig. 13—Crack speed history for a crack propagating dynamically in a graphite/epoxy composite plate